

Ohmic-to-Schottky Conversion in Monolayer Tellurene–Metal Interface via Graphene Insertion

Sanchali Mitra, Om Kesharwani, and Santanu Mahapatra*

Cite This: *J. Phys. Chem. C* 2021, 125, 12975–12982

Read Online

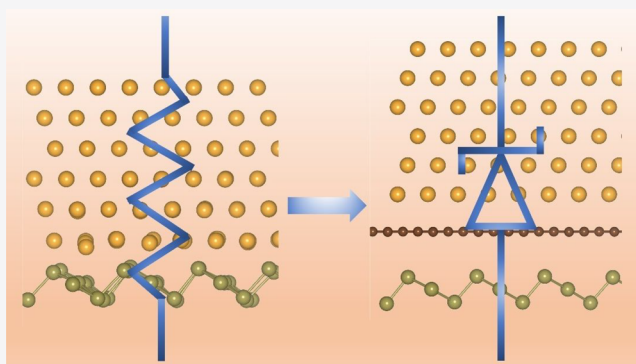
ACCESS |

Metrics & More

Article Recommendations

Supporting Information

ABSTRACT: Tellurene, a relatively new addition to the two-dimensional (2D) material family, has shown promising prospect in future nanoelectronics. Atomistic understanding of the electronic properties of 2D material–metal interfaces is crucial to promote optimal device performance. Monolayer tellurene exhibits an unusual Ohmic nature when interfaced with any metal surfaces, restricting its applications in vertical Schottky barrier devices. Using density functional theory (DFT), here, we describe a technique of adding a buffer layer to prevent the formation of Ohmic contact. Using six different metals (Ag, Au, Pt, Pd, Ru, and Ti), we show that the insertion of a graphene layer between tellurene and a metal surface can screen the metallization of tellurene and create Schottky barriers. The Schottky barrier heights (SBHs) can be now modulated using metal electrodes with different work functions (WFs) because the graphene layer partially depins the Fermi level. Our study provides quantum-chemical insights into the realization of vertical Schottky diodes using monolayer tellurene that could be a key component in future high-frequency nanoelectronic devices.



INTRODUCTION

Two-dimensional (2D) layered materials have emerged as promising candidates for next-generation electronic and optoelectronic devices because of their atomic-scale thickness, tunable electronic characteristics, mechanical flexibility, and strong light–matter interactions.^{1–3} The heterostructures formed by contacting 2D materials with other 2D materials or bulk metals have attracted special attention for applications in next-generation flexible and wearable electronics.^{4–6} These heterostructures usually lead to two types of contacts: Ohmic with linear I–V relationship and Schottky with nonlinear I–V characteristics. 2D material-based Schottky heterojunctions are now being investigated for applications in transistors, rectifiers, logic gates, sensors, memory devices, and so on.^{7–9} From a plethora of 2D materials, researchers are focusing on forming heterostructures with a new 2D material family.

Recently, as a new member of 2D material family, the existence of group VI tellurene (2D Tellurium) in its monolayer (ML) and few-layer form has been confirmed by experimental work and theoretical calculations.^{10–12} Bulk tellurium possesses monoclinic (named α -Te),¹³ trigonal (β -Te),¹⁴ and tetragonal symmetries among which β -Te is the most stable in an ambient environment. Tellurene has a layer-dependent band gap; bulk β -Te has a narrow band gap of about 0.35 eV, while in ML Te, the band gap increases to about 1.25 eV.¹⁵ Tellurene has great potential applications in nanodevices because of its favorable properties such as high carrier mobility, excellent light absorption, superb thermo-

electric performance, and good stability at room temperature.^{16–19} Recently, the interfacial characteristics of tellurene with a series of metals and graphene have been reported.²⁰ It was shown that tellurene was metallized while contacting with metals; hence, no vertical Schottky contacts can be made with ML tellurene. However, vertical Schottky devices exhibit several advantages over their counterpart lateral devices, such as ultrafast charge transfer, scaling down device dimensions to an atomic level, and precise tuning of the energy band alignment.^{21,22}

In the present study, we explore a technique to create vertical Schottky barriers at the ML tellurene–metal interface. Previous investigations have reported that inserting a graphene layer between a 2D semiconductor and metal allowed the modulation of Schottky barrier heights (SBHs).^{23–25} Several theoretical and experimental studies demonstrated SBH reduction and Fermi-level pinning in graphene-inserted MoS₂–metal interfaces.^{25–27} Inspired by these studies, we have attempted to find out the consequence of graphene insertion between ML tellurene and metal surfaces. Surpris-

Received: March 26, 2021

Revised: May 22, 2021

Published: June 7, 2021



Table 1. Calculated Interlayer Properties of ML Tellurene–Metal and Tellurene–Graphene–Metal Contacts^a

system	Au-Te	Ag-Te	Pd-Te	Pt-Te	Ru-Te	Ti-Te	C-Te	Au-C-Te	Ag-C-Te	Pd-C-Te	Pt-C-Te	Ru-C-Te	Ti-C-Te
total number of atoms	180	180	273	144	129	222	96	258	258	396	200	200	353
$\bar{\epsilon}$ (%)	0.80	0.61	0.45	0.54	0.70	0.62	0.61	0.30	0.80	0.50	0.49	0.52	1.97
d_z (Å)	2.28	2.20	2.16	2.1	2.13	2.13	3.38	$d_1 = 3.04$ $d_2 = 3.67$	$d_1 = 3.11$ $d_2 = 3.44$	$d_1 = 3.48$ $d_2 = 3.48$	$d_1 = 3.16$ $d_2 = 3.45$	$d_1 = 3.36$ $d_2 = 3.36$	$d_1 = 2.15$ $d_2 = 3.22$
E_b (eV)	-1.86	-2.19	-4.4	-4.32	-4.92	-6.88	-0.3	-0.9	-0.94	-1.12	-1.36	-1.04	-3.41

^a $\bar{\epsilon}$ is the average lattice constant mismatch between ML tellurene and the metal/metal–graphene surface. d_z is the average vertical distance between the contact layers of tellurene and metal. E_b is the average binding energy.

ingly, we found that the sandwiched graphene layer acts as a buffer that prevents the metallization of tellurene, creating a vertical Schottky barrier. Utilizing density functional theory (DFT), we have evaluated the geometries, electronic properties, and charge transfer across the interfaces of ML tellurene–graphene–metal heterostructures. We have employed six metals (Au, Ag, Pd, Pt, Ru, and Ti) with a wide range of workfunctions (WFs), which are commonly used as electrode materials. Unlike the previous reported studies²⁵ on 2D semiconductor (like MoS₂)–metal interfaces where graphene was usually used to pin the Fermi level, this study reveals the Fermi-level depinning for Ohmic-to-Schottky conversion using the graphene insertion technique.

COMPUTATIONAL DETAILS

Geometry relaxation has been carried out using the Vienna ab-initio simulation package (VASP)^{28–30} with the projector-augmented wave (PAW) method³¹ and generalized gradient approximation–Perdew–Burke–Ernzerhof (GGA–PBE)³² exchange correlation functional. A sufficiently large cutoff energy of 520 eV is used to avoid Pulay stress. For all structural relaxation, $\frac{30}{a} \times \frac{30}{b} \times \frac{30}{c}$ Monkhorst–Pack k-points grids³³ are used to sample the Brillouin zone, where a , b , and c are the lengths of the lattice parameters of a supercell. As electronic convergence criteria, the energy difference in successive iterations was set to 10^{-6} eV. The Gaussian smearing method was used with a smearing width of 0.05 eV. The structural geometry was optimized until the Hellmann–Feynman force on every atom falls below 0.01 eV/Å. Two corrections were considered in all calculations. One is the van der Waals interaction with the zero damping DFT-D3 method of Grimme^{34,35} and the other is the dipole correction applied to eliminate the pseudo-interaction of the dipole moments caused by periodicity in the z-direction.

For the calculations of electronics properties, we used Quantum ATK³² instead of VASP because of some discrepancies raised in the projected band calculations in the VASP. These are discussed in detail in the Results and Discussion section. The SG15 norm conserving pseudopotentials^{36,37} were employed along with the linear combination of atomic orbital (LCAO) basis sets of “medium” accuracy. Van der Waals interactions with the zero damping DFT-D3 method of Grimme were used. A denser $\frac{60}{a} \times \frac{60}{b} \times \frac{60}{c}$ k mesh was chosen, and a cutoff energy of 185 Ha was used for these static calculations. The Gaussian smearing method with an electron temperature of 600 K was used.

For the interface design, six layers of <111>-cleaved surfaces of Au, Ag, Pd, and Pt and <0001>-cleaved surfaces of Ru and Ti are considered. To create an interface, the supercells of two

surfaces are aligned and matched by applying strain on one or both surfaces. Large supercells can minimize the lattice mismatch between the two surfaces. In a recent work²⁰ on tellurene–metal interfaces, the interface strain is quite high (above 2%); even for some metals, it is about 5%. Sometimes, such high strain may alter the electronic properties of the heterostructures. Therefore, in this work, we have used large supercells to make the interface strain below 1% for all the metals. The interfaces are built with a QuantumATK interface builder³⁸ module. All the details regarding the interface building, including the supercell size, surface rotation angle, and strain tensor are given in Supplementary Table 1. In Table 1, the mean interface strain and the number of atoms in each heterostructure are listed. A vacuum layer of 20 Å was added to eliminate any spurious interaction between two periodic replicas. During DFT simulations, the top three layers of metal atoms toward the vacuum side were fixed to emulate the feature of bulk electrodes.

RESULTS AND DISCUSSION

Tellurene–Metal Interface. Interface Geometry. The relaxed structure of ML β tellurene is composed of six-membered chairlike rings and four-membered planar rings (Figure 1a). The optimized lattice parameters $a = 4.22$ Å and $b = 5.61$ Å and obtained two Te–Te bond distances $x_1 = 2.76$ Å and $x_2 = 3.01$ Å are in good accordance with the reported value.^{15,20}

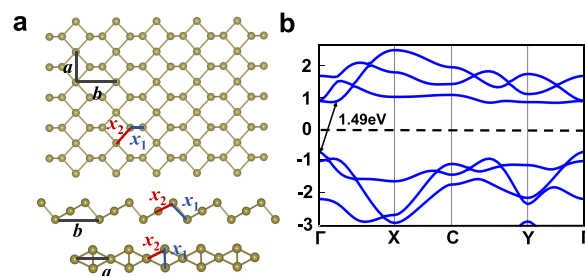


Figure 1. (a) Top and side views of pristine ML tellurene. The calculated lattice parameters are $a = 4.22$ Å and $b = 5.61$ Å. Te–Te bond distances are $x_1 = 2.76$ Å and $x_2 = 3.01$ Å. (b) Energy band structure of ML tellurene showing an indirect band gap of 1.49 eV. Black dashed line represents the Fermi level.

The relaxed geometries of ML tellurene–metal interfaces are shown in Figure 2. The structure of ML tellurene distorts slightly while interfacing with Au and Ag. However, for the other four metals, there is a strong change in the tellurene structure; especially for Ti, the structure completely destroyed. The mean strain of the interfaces, vertical average distance (d_z) between the top layers of tellurene and the bottom layers of

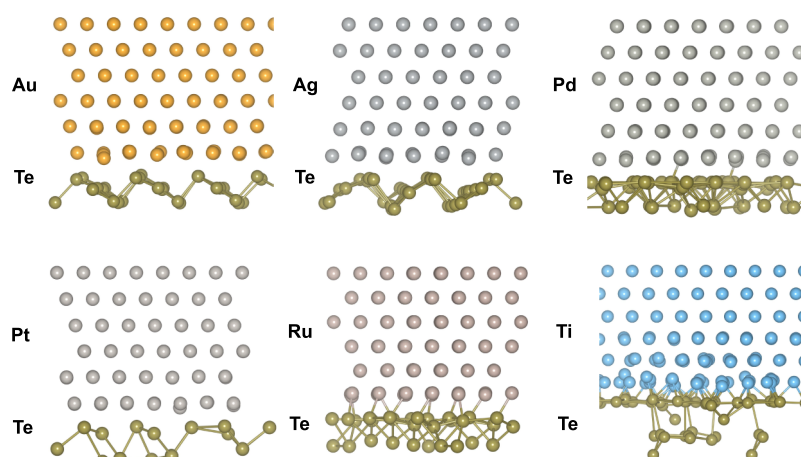


Figure 2. Side view of the relaxed structures of ML tellurene interfaced with Au, Ag, Pd, Pt, Ru, and Ti surfaces.

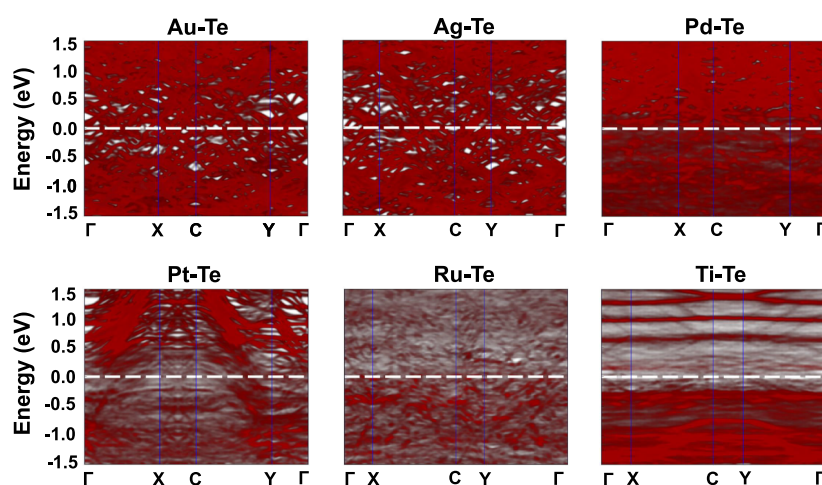


Figure 3. Energy band diagrams of ML tellurene–metal systems. Red lines denote the bands projected to tellurene. Fermi level is located at zero energy and is represented by white dashed lines.

metals, and binding energies are listed in Table 1. The average binding energy is defined as follows:

$$E_b^{\text{MTe}} = (E_{\text{MTe}} - E_M - E_{\text{Te}}) / N \quad (1)$$

where E_{MTe} , E_M , and E_{Te} are the total energies of tellurene–metal systems, pure metal surfaces, and pure tellurene, respectively. N is the number of tellurene atoms in the topmost layer that are in direct contact with metal atoms. Tellurene interactions on the metal surfaces can be classified into two types according to the binding energy values. On Au and Ag, adhesion is moderate with a binding energy value in the range $-2.5 < E_b < -1.5$ eV. On the other four metal surfaces, the adhesion is strong with a binding energy < -4 eV. The binding energy is most negative in the tellurene–Ti interface where structural distortion is also maximum. The difference in bonding strength may arise from different numbers of unpaired electrons in metals. Au ($5d^{10}6s^1$) and Ag ($4d^{10}5s^1$) only have one unpaired electron in their outermost orbitals, whereas Pd ($4d^95s^1$) and Pt ($5d^96s^1$) have two, and Ru ($4d^75s^1$) and Ti ($3d^34s^1$) have four unpaired electrons. Therefore, tellurene atoms form a smaller number of covalent bonds with Au and Ag compared to other metals.

Band Structure Analysis. In Figure 3, the projected band structures of tellurene in the tellurene–metal systems are plotted. From our simulations, we obtain that pure ML

tellurene has an indirect band gap of 1.49 eV (Figure 1b) that is close to the other reported data.³⁹ While interfacing with metals, the band structure of tellurene completely destroyed, implying chemisorption of tellurene on all metal surfaces. Some bands always cross the Fermi level, indicating metallization of tellurene. On all the metal surfaces, tellurene becomes metallic from semiconducting. This phenomenon is quite different from other 2D semiconducting materials like MoS_2 , WS_2 , and ReS_2 , where both the Ohmic and Schottky nature of contacts were observed.^{25,40,41} To compare the chemical reactivity of these materials, we have evaluated the electron localization functions (ELFs)⁴² of these 2D materials. The ELF introduced by Becke and Edgecombe has been proven to be a valuable tool to determine the location of electron pairs. The existence of a localized electron pair implies that there is a high probability of finding two electrons of opposite spin in a given space, and hence, the probability of exchange with other electrons outside of this space is small. High ELF values show that the electrons are more localized at the examined position than in a uniform electron gas of the same density. The ELF of ML tellurene has a low peak value compared to other 2D materials (Supplementary Figure 1), implying the electron density is more delocalized in tellurene, and hence, it is more reactive, forming metallic nature of ML tellurene while interfacing with any metal.

Schottky Barrier Analysis. Figure 4a shows the schematic diagram of Schottky junctions formed in ML tellurene–metal–

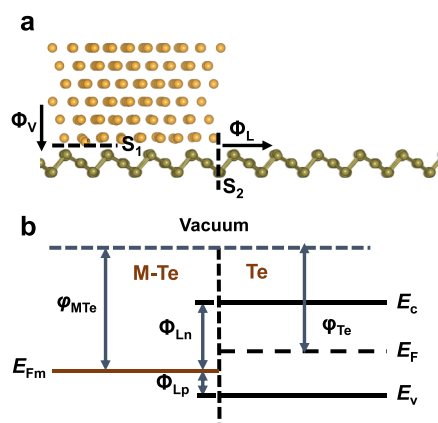


Figure 4. (a) Schematic diagram of vertical and lateral contacts formed between metal and ML tellurene. Φ_v and Φ_L denote vertical and lateral SBHs between the metal–tellurene interface, respectively. Black arrow shows the direction of charge carrier flow. (b) Schematic energy band diagram at the lateral junction formed between the combined metal–tellurene system (M–Te) and pristine tellurene (Te). E_c and E_v denote the energies of the conduction band (CB) and valence band (VB) of pristine tellurene nearest to the Fermi level. E_f and E_{fM} represent the Fermi levels of pristine tellurene and the combined metal–tellurene system.

based typical semiconducting devices. As depicted in the figure, two distinct interfaces are formed: one is the vertical interface between metal and tellurene (S_1) and another is the lateral interface formed between the contacted tellurene and pristine tellurene (S_2). According to tellurene-projected band structure analysis, ML tellurene forms an Ohmic contact with metal owing to its metallization. Therefore, for all metals, SBHs (Φ_v) between metal–tellurene vertical interfaces are zero. The Schottky barrier across the lateral interface can be formed because of the work function difference between the combined metal–tellurene system and pristine tellurene. The Schottky Mott rule may be used to evaluate the lateral SBH (Φ_L). To find out Φ_L , the WF of the combined metal–tellurene system and pristine tellurene is calculated using DFT, and the vacuum levels of the two are aligned (Figure 4b). According to the Schottky Mott rule, the p-type and n-type Schottky barriers are defined as follows:

$$\Phi_{Ln} = \varphi_{MTe} - E_c \quad (2)$$

$$\Phi_{Lp} = E_v - \varphi_{MTe} \quad (3)$$

where φ_{MTe} is the WF of the combined metal–tellurene system, and E_c and E_v are energies corresponding to conduction band minima (CBM) and valence band maxima (VBM) of pristine tellurene.

Figure 5 shows the WFs of metal–tellurene systems along with the CB and VB energies of pristine tellurene. In QuantumATK, the WFs are calculated using the “ghost atom” technique.⁴³ Pristine metal WFs calculated using this technique match well with the reported data.²⁵ Because there are limited studies on metal–tellurene systems, we have calculated all the WFs using VASP and compared with the ATK data. The results are in good accordance with each other (Supplementary Table 2). If the WF of the combined system is below the VBM or above the CBM of pristine tellurene, the

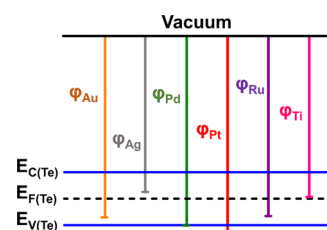


Figure 5. Representation of the WF of the combined metal–tellurene system with respect to the CBM and VBM of pristine tellurene across the lateral junction shown in Figure 4. If the metal WF is between the CBM and Fermi level, the contact is n-type, and if the metal WF is between the Fermi level and VBM, the contact is p-type. If the WF is lower than the CBM and higher than the VBM, Ohmic contact forms.

lateral contact is Ohmic, and if it falls within the band gap, Schottky contact forms. ML tellurene forms n-type lateral Schottky contacts with Ag and Ti, while p-type Schottky contacts with Au and Ru. For Pd and Pt, the contacts are Ohmic. In Table 2, the WFs of metals, combined metal–

Table 2. Evaluation of Lateral Schottky Barriers across Metal–Tellurene interface^a

structure	φ_M (eV)	φ_{MTe} (eV)	Φ_{Ln} (eV)	Φ_{Lp} (eV)
Au–Te	5.11	5.12		0.63
Ag–Te	4.495	4.4	0.19	
Pd–Te	5.305	5.35	ohmic	ohmic
Pt–Te	5.65	5.61	ohmic	ohmic
Ru–Te	5.01	5.08		0.49
Ti–Te	4.49	4.54	0.05	

^a φ_M and φ_{MTe} denote DFT-calculated WFs of the pristine metal surface and metal–tellurene composite system; Φ_{Ln} and Φ_{Lp} denote n-type and p-type lateral SBHs, respectively.

tellurene systems, and corresponding lateral SBH are listed. According to the metal WF values, metals leading to lower WFs (Ag and Ti) form n-type Schottky contacts, whereas metals with higher WFs (Au and Ru) form p-type Schottky contacts, and metals with large WFs (Pd and Pt) form Ohmic contacts. The heights of the Schottky barrier also increase with increasing metal WFs.

Graphene-Inserted Tellurene–Metal Interface. To build a vertical Schottky device, the metallization of tellurene on the metal surfaces must be screened. Yan et al. have shown that the band structure of ML tellurene is preserved well on graphene surface.²⁰ To verify this, we have also designed an ML tellurene–graphene interface with an interface strain below 1% and evaluated its electronic properties. The binding energy of tellurene on graphene is quite low compared to other metals (Table 1), and also, the interlayer distance is large, implying weak van der Waals interactions. Unlike metals, tellurene band gaps remain unchanged while interfacing with graphene. The Fermi level comes very close to the VB of tellurene, implying the formation of p-type Schottky contact, but the SBH is extremely low. Owing to the physisorption of tellurene on the graphene surface, sandwiching a graphene layer between tellurene and metal may screen the hybridization of tellurene and prevent its metallization.

Interface Design. To design the tellurene–graphene–metal heterostructures, initially, the interface between metal and graphene layers are created, and the supercell of the combined graphene–metal surface is matched with the supercell of ML

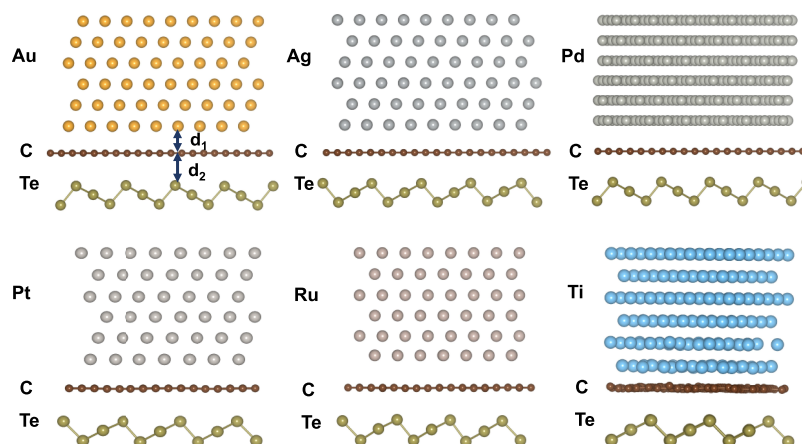


Figure 6. Side view of relaxed geometries of metal–graphene–ML tellurene heterostructures. d_1 and d_2 denote average vertical distances between the bottom metal layer and graphene; and graphene and top tellurene layer, respectively.

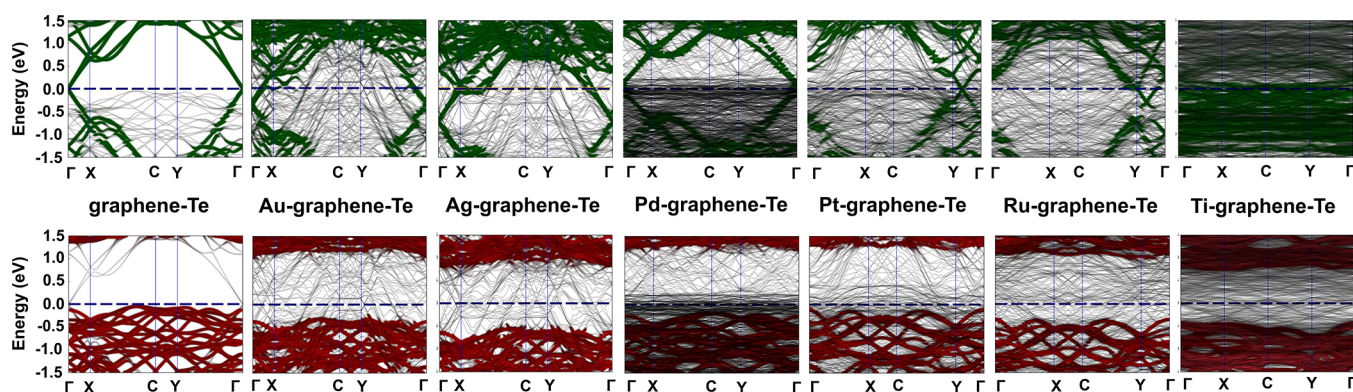


Figure 7. Band structures of tellurene–graphene–metal heterostructures. In the upper panel, projected band structures of graphene and in the lower panel, projected band structures of tellurene are shown. Gray lines represent total bands, green and red lines represent bands projected to graphene and tellurene, respectively. Fermi level is set at zero energy and denoted by blue dashed lines.

tellurene. To minimize the strain, large supercells are used. The relaxed geometries are displayed in Figure 6. The mean interface strains, interlayer distances, and binding energies are listed in Table 1. The binding energy of the graphene-inserted system is calculated as follows:

$$E_b^{\text{MCTe}} = (E_{\text{MCTe}} - E_{\text{M}} - E_{\text{C}} - E_{\text{Te}})/N \quad (4)$$

where E_{MCTe} , E_{M} , E_{C} , and E_{Te} are the total energies of tellurene–graphene–metal systems, pure metal surfaces, pure graphene, and pure tellurene, respectively, and N is the number of tellurene atoms directly contacted with graphene.

The average binding energy of tellurene in the graphene-inserted system is quite low compared to that of the pure metal system. The binding energy of the tellurene–graphene–Ti system is more negative compared to other metals. More negative binding energy means a more stable structure with a greater number of chemical bonds. In all the composite systems, the tellurene structure remains unchanged, implying the physisorption of tellurene. However, the structure of graphene is little distorted at the Ti interface and preserved on other metals. According to the relaxed geometries and binding energy values, graphene is chemisorbed on Ti and physisorbed on the rest of the metals. Projected band structure analysis will give more insights into the chemisorption and physisorption of graphene on different metal surfaces.

Band Structure Analysis. The projected band structures of both graphene and tellurene in tellurene–graphene–metal heterostructures are shown in Figure 7. For the tellurene–graphene system, the Dirac cone is visible at the Γ point. The shift of the Dirac point from the K point to the Γ point is due to band folding in supercells. For tellurene–graphene–metal systems, the Dirac points of graphene are preserved for Au, Ag, and Pd but shifted with respect to the Fermi level. For Ru and Pt, the band structures of graphene are perturbed slightly, but still the Dirac point is visible between Y and Γ paths, while at the Ti interface, the band structure became completely perturbed, implying the chemisorption of graphene on Ti.

From the projected band structure of tellurene, we found that the semiconducting nature of tellurene remains preserved in all the heterostructures, only the energy bands are shifted with respect to the Fermi level, creating vertical Schottky barriers between the tellurene and graphene–metal interface. Regarding the shift, we found discrepancies in the projected band calculations using VASP and ATK. From VASP calculations, we found that for Au, Pd, Pt, and Ru, the VBs of tellurene come near the Fermi level, making p-type Schottky contact, whereas for Ag and Ti, the CBs of tellurene are near the Fermi level, forming an n-type Schottky contact (Supplementary Figure 2). However, from QuantumATK simulations, we observed that tellurene builds p-type Schottky contacts with all graphene-inserted metal surfaces. To explain such discrepancies, we have performed Bader charge analysis⁴⁴

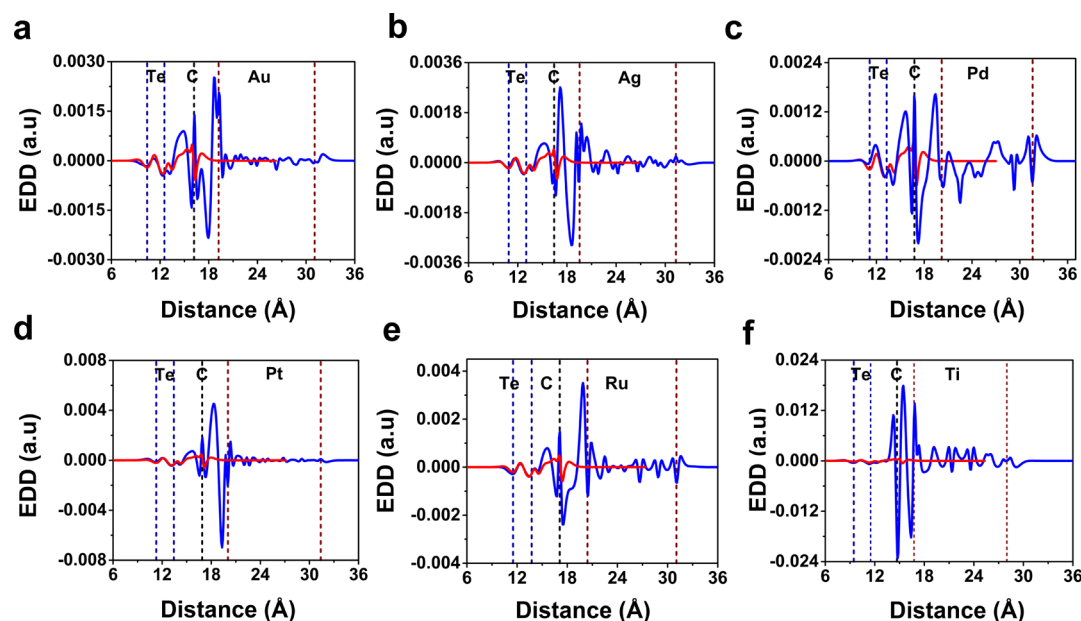


Figure 8. Electron density difference (EDD) for (a) tellurene–graphene–Au, (b) tellurene–graphene–Ag, (c) tellurene–graphene–Pd, (d) tellurene–graphene–Pt, (e) tellurene–graphene–Ru, and (f) tellurene–graphene–Ti heterostructures. The red line superimposed on each graph represents EDD for the tellurene–graphene system.

in these heterosystems using VASP. According to the calculated Bader charge (Supplementary Table 3), the total charge of tellurene in all the heterostructures is less than that of pristine tellurene, that is, charge depletion takes place with interfacing tellurene with graphene–metal surfaces, implying p-type nature. The Bader charge analysis contradicts the projected band calculations performed by VASP itself but validates the QuantumATK results. The atom-projected states are calculated by projecting the WF onto localized atomic orbitals. In VASP, for the projection calculation, the radius of a sphere around the atom is set to cut off the projection. The discrepancy may arise because of some projection loss in VASP. As QuantumATK use localized atomic orbital basis, the evaluation of the atom-projected state is more accurate than VASP.

Charge-Transfer Investigation. The generation of Schottky barriers is further explored by evaluating the electron density difference (EDD) and Mulliken population analysis calculated using QuantumATK. For the tellurene–graphene–metal interface, the EDD is defined as

$$\Delta\rho = \rho_{\text{MCTe}} - \rho_{\text{M}} - \rho_{\text{C}} - \rho_{\text{Te}} \quad (5)$$

where ρ is the electron density.

The EDD plots are shown in Figure 8. Blue lines denote the EDD averaged along the z-direction of tellurene–graphene–metal heterostructures. The EDD of the graphene–tellurene system is shown by the red line superimposed on each graph. Both charge accumulation and depletion regions are found at the interfaces. These charge redistributions lead to further dipole formation at interfaces that results in band alignment. Comparing the EDD at the graphene–metal interface, charge transfer is very high for Ti compared to other metals, implying chemisorption of graphene on Ti. At the tellurene–graphene interface, the electron density is negative at the tellurene side while it is positive at the graphene side, implying electron transfer from tellurene to graphene. To understand the charge transfer at tellurene, we have calculated the area under the

EDD graph in the entire tellurene region (Table 3). The positive area implies more accumulation while negative means

Table 3. Heights of Vertical Schottky Barriers and Charge Analysis at ML Tellurene and Graphene–Metal Interfaces. Φ_{Vn} and Φ_{Vp} Denote n-Type and p-Type SBHs, Respectively^a

structure	Φ_{Vn} (eV)	Φ_{Vp} (eV)	EDD area ($\times 10^{-4} \text{ \AA}^2$)	Q_{Te} (e)	Q_{MCTe} (e)	Δ_Q (e)
C-Te	1.35	0.047	−3.9878	368	367.674	−0.326
Au-C-Te	1.1	0.32	−5.0515	384	383.695	−0.305
Ag-C-Te	0.82	0.57	−4.1354	384	383.648	−0.352
Pd-C-Te	1.25	0.195	−3.6106	576	575.627	−0.373
Pt-C-Te	1.28	0.12	−4.3180	288	287.772	−0.228
Ru-C-Te	1.0	0.35	−4.7704	288	287.684	−0.352
Ti-C-Te	0.7	0.6	−8.1512	528	527.274	−0.726

^aEDD area means the area under the EDD curve in the tellurene region. Q_{Te} and Q_{MCTe} represent Mulliken charges in pristine tellurene and tellurene layers in the composite system, respectively. $\Delta_Q = Q_{\text{MCTe}} - Q_{\text{Te}}$. Negative values of Δ_Q imply depletion of charge in tellurene when interfaced with a graphene–metal surface.

depletion. For all the heterostructures, the area is negative inside the tellurene region. Therefore, contacting tellurene with the graphene–metal interface depletion of charge occurs at tellurene transforming it into p-type. The same is verified using the Mulliken population analysis.⁴⁵ The Mulliken charges of tellurene in its pristine form and in the tellurene–graphene–metal heterostructures are listed in Table 3. In all the composite systems, the Mulliken charge in the tellurene layer is less than the charge in the pristine tellurene alluding the depletion of charge.

Schottky Barrier Analysis. Pure tellurene is an intrinsic semiconductor; while interfacing with a graphene–metal surface, the VBs of tellurene come close to the Fermi level, converting it into p-type. The height of the p-type Schottky

barrier has been evaluated by taking the energy difference between the Fermi level and VBM from the tellurene-projected band structure. The SBH is lowest for pure graphene–tellurene interface (Table 3). In the tellurene–graphene–metal system, the shift of the VB is maximum for Pt, suggesting maximum charge transfer. However, the EDD area and Mulliken charge do not depict the same. The charge analysis cannot quantitatively explain the change in SBH but accurately describe the p-type or n-type nature of contacts. There is, however, a correlation between the change in the SBH and WF of metal. In Figure 9, we have plotted the change in the SBH

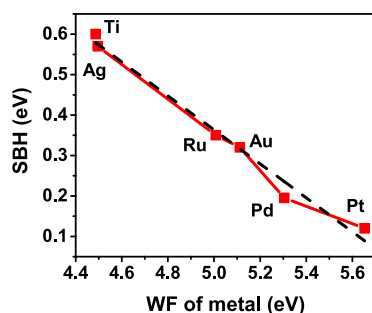


Figure 9. Plot showing p-type vertical SBHs at tellurene and graphene–metal interface with respect to the WFs of six investigated metals.

with the metal WF. With increasing WFs the SBH reduces almost linearly. When tellurene makes contact with pure metals, its band gap diminishes, and the barrier nature becomes utterly insensitive of the metals. Graphene insertion not only preserves the semiconducting nature of tellurene but also makes the barrier height dependent on the metal WF. This phenomenon is similar to “Fermi-level depinning.” Fitting the WF–SBH characteristic curve with the linear equation, we obtain a straight line of slope 0.41 that can be considered as the Fermi-level depinning factor.

CONCLUSIONS

In summary, this study demonstrates a simple technique to convert Ohmic contacts between ML tellurene and metal surfaces into Schottky contacts. Using rigorous DFT simulations, we have found that tellurene is chemisorbed on most of the metal surfaces that are commonly used as electrodes in experimental devices. When the tellurene–metal interface is formed, because of strong chemical bonding the semiconducting nature of tellurene is destroyed, and it becomes metallic. Therefore, only Ohmic contacts can be formed vertically between tellurene and metal surfaces. However, by inserting a graphene layer between the two surfaces, the semiconducting nature of tellurene can be preserved. Because of weak van der Waals interactions between graphene and tellurene, graphene acts as a buffer layer that prevents the chemical bond formation between metal and tellurene, eliminating metallization. For all the six investigated metals (Au, Ag, Pd, Pt, Ru, and Ti), we found p-type Schottky barriers at tellurene and graphene–metal interfaces. The barrier height is dependent on the metal WF; as the metal WF decreases, the SBH increases. Therefore, graphene insertion leads to depinning of the Fermi level in ML tellurene–metal interface, creating vertical Schottky barriers in which barrier heights can be tuned by changing metal electrodes. This study is extremely useful in realizing vertical

Schottky barrier diodes using ML tellurene, a newly invented high-mobility 2D semiconductor for future high-frequency nanoelectronic devices.

ASSOCIATED CONTENT

Supporting Information

The Supporting Information is available free of charge at <https://pubs.acs.org/doi/10.1021/acs.jpcc.1c02723>.

Details of the interface building, comparison between VASP and QuantumATK WF calculations, Bader charge analysis, electron localization function, and projected band structure of tellurene (PDF).

AUTHOR INFORMATION

Corresponding Author

Santanu Mahapatra – Nano-Scale Device Research Laboratory, Department of Electronic Systems Engineering, Indian Institute of Science (IISc) Bangalore, Bangalore 560012, India; orcid.org/0000-0003-1112-8109; Email: santanu@iisc.ac.in

Authors

Sanchali Mitra – Nano-Scale Device Research Laboratory, Department of Electronic Systems Engineering, Indian Institute of Science (IISc) Bangalore, Bangalore 560012, India

Om Kesharwani – Nano-Scale Device Research Laboratory, Department of Electronic Systems Engineering, Indian Institute of Science (IISc) Bangalore, Bangalore 560012, India

Complete contact information is available at: <https://pubs.acs.org/doi/10.1021/acs.jpcc.1c02723>

Notes

The authors declare no competing financial interest.

ACKNOWLEDGMENTS

Authors acknowledge Arnab Kabiraj, Nano-Scale Device Research Laboratory, IISc Bangalore, for valuable discussions regarding DFT calculations. This work was supported by the Mathematical Research Impact Centric Support (MATRICS) scheme of Science and Engineering Research Board (SERB), Government of India, under Grant No. MTR/2019/000047. S. Mitra acknowledges IISc Institute of Eminence (IOE) postdoctoral fellowship for financial support.

REFERENCES

- (1) Lin, Z.; McCreary, A.; Briggs, N.; Subramanian, S.; Zhang, K.; Sun, Y.; Li, X.; Borys, N. J.; Yuan, H.; Fullerton-Shirey, S. K.; Chernikov, A.; Zhao, H.; McDonnell, S.; Lindenberg, A. M.; Xiao, K.; LeRoy, B. J.; Drndić, M.; Hwang, J. C. M.; Park, J.; Chhowalla, M.; Schaak, R. E.; Javey, A.; Hersam, M. C.; Robinson, J.; Terrones, M. 2D Materials Advances: From Large Scale Synthesis and Controlled Heterostructures to Improved Characterization Techniques, Defects and Applications. *2D Mater.* **2016**, *3*, No. 42001.
- (2) Yu, W. J.; Li, Z.; Zhou, H.; Chen, Y.; Wang, Y.; Huang, Y.; Duan, X. Vertically Stacked Multi-Heterostructures of Layered Materials for Logic Transistors and Complementary Inverters. *Nat. Mater.* **2013**, *12*, 246–252.
- (3) Wang, Q. H.; Kalantar-Zadeh, K.; Kis, A.; Coleman, J. N.; Strano, M. S. Electronics and Optoelectronics of Two-Dimensional Transition Metal Dichalcogenides. *Nat. Nanotechnol.* **2012**, *7*, 699–712.

- (4) Dong, R.; Zhang, T.; Feng, X. Interface-Assisted Synthesis of 2D Materials: Trend and Challenges. *Chem. Rev.* **2018**, *118*, 6189–6235.
- (5) Schulman, D. S.; Arnold, A. J.; Das, S. Contact Engineering for 2D Materials and Devices. *Chem. Soc. Rev.* **2018**, *47*, 3037–3058.
- (6) Lee, C.-H.; Lee, G.-H.; van der Zande, A. M.; Chen, W.; Li, Y.; Han, M.; Cui, X.; Arefe, G.; Nuckolls, C.; Heinz, T. F.; Guo, J.; Hone, J.; Kim, P. Atomically Thin p–n Junctions with van Der Waals Heterointerfaces. *Nat. Nanotechnol.* **2014**, *9*, 676–681.
- (7) Zhang, X.; Liu, B.; Gao, L.; Yu, H.; Liu, X.; Du, J.; Xiao, J.; Liu, Y.; Gu, L.; Liao, Q.; Kang, Z.; Zhang, Z.; Zhang, Y. Near-Ideal van Der Waals Rectifiers Based on All-Two-Dimensional Schottky Junctions. *Nat. Commun.* **2021**, *12*, 1522.
- (8) Lv, L.; Yu, J.; Hu, M.; Yin, S.; Zhuge, F.; Ma, Y.; Zhai, T. Design and Tailoring of Two-Dimensional Schottky, PN and Tunneling Junctions for Electronics and Optoelectronics. *Nanoscale* **2021**, 6713.
- (9) Gong, F.; Fang, H.; Wang, P.; Su, M.; Li, Q.; Ho, J. C.; Chen, X.; Lu, W.; Liao, L.; Wang, J.; Hu, W. Visible to Near-Infrared Photodetectors Based on MoS₂ vertical Schottky Junctions. *Nanotechnology* **2017**, *28*, 484002.
- (10) Wang, Y.; Qiu, G.; Wang, R.; Huang, S.; Wang, Q.; Liu, Y.; Du, Y.; Goddard, W. A.; Kim, M. J.; Xu, X.; Ye, P. D.; Wu, W. Field-Effect Transistors Made from Solution-Grown Two-Dimensional Tellurene. *Nat. Electron.* **2018**, *1*, 228–236.
- (11) Qiu, G.; Wang, Y.; Nie, Y.; Zheng, Y.; Cho, K.; Wu, W.; Ye, P. D. Quantum Transport and Band Structure Evolution under High Magnetic Field in Few-Layer Tellurene. *Nano Lett.* **2018**, *18*, 5760–5767.
- (12) Cai, X.; Han, X.; Zhao, C.; Niu, C.; Jia, Y. Tellurene: An Elemental 2D Monolayer Material beyond Its Bulk Phases without van Der Waals Layered Structures. *J. Semicond.* **2020**, *41*, No. 081002.
- (13) Takumi, M.; Masamitsu, T.; Nagata, K. X-Ray Structural Analysis of the High-Pressure Phase III of Tellurium. *J. Phys. Condens. Matter* **2002**, *14*, 10609–10613.
- (14) Bureau, B.; Boussard-Pledel, C.; Lucas, P.; Zhang, X.; Lucas, J. Forming Glasses from Se and Te. *Molecules* **2009**, 4337.
- (15) Wu, B.; Liu, X.; Yin, J.; Lee, H. Bulk β -Te to Few Layered β -Tellurenes: Indirect to Direct Band-Gap Transitions Showing Semiconducting Property. *Mater. Res. Express* **2017**, *4*, 95902.
- (16) Lin, C.; Cheng, W.; Chai, G.; Zhang, H. Thermoelectric Properties of Two-Dimensional Selenene and Tellurene from Group-VI Elements. *Phys. Chem. Chem. Phys.* **2018**, *20*, 24250–24256.
- (17) Wines, D.; Kropp, J. A.; Chaney, G.; Ersan, F.; Ataca, C. Electronic Properties of Bare and Functionalized Two-Dimensional (2D) Tellurene Structures. *Phys. Chem. Chem. Phys.* **2020**, *22*, 6727–6737.
- (18) Deckoff-Jones, S.; Wang, Y.; Lin, H.; Wu, W.; Hu, J. Tellurene: A Multifunctional Material for Midinfrared Optoelectronics. *ACS Photonics* **2019**, *6*, 1632–1638.
- (19) Cai, X.; Jia, X.; Liu, Y.; Zhang, L.; Yu, W.; Wang, B.; Yang, X.; Wang, Q.; Jia, Y. Enhanced Carrier Mobility and Tunable Electronic Properties in α -Tellurene Monolayer via an α -Tellurene and h-BN Heterostructure. *Phys. Chem. Chem. Phys.* **2020**, *22*, 6434–6440.
- (20) Yan, J.; Zhang, X.; Pan, Y.; Li, J.; Shi, B.; Liu, S.; Yang, J.; Song, Z.; Zhang, H.; Ye, M.; Quhe, R.; Wang, Y.; Yang, J.; Pan, F.; Lu, J. Monolayer Tellurene–Metal Contacts. *J. Mater. Chem. C* **2018**, *6*, 6153–6163.
- (21) Yang, S. J.; Park, K.-T.; Im, J.; Hong, S.; Lee, Y.; Min, B.-W.; Kim, K.; Im, S. Ultrafast 27 GHz Cutoff Frequency in Vertical WSe₂ Schottky Diodes with Extremely Low Contact Resistance. *Nat. Commun.* **2020**, *11*, 1574.
- (22) Nazir, G.; Kim, H.; Kim, J.; Kim, K. S.; Shin, D. H.; Khan, M. F.; Lee, D. S.; Hwang, J. Y.; Hwang, C.; Suh, J.; Eom, J.; Jung, S. Ultimate Limit in Size and Performance of WSe₂ Vertical Diodes. *Nat. Commun.* **2018**, *9*, 5371.
- (23) Du, Y.; Yang, L.; Zhang, J.; Liu, H.; Majumdar, K.; Kirsch, P. D.; Ye, P. D. MoS₂ Field-Effect Transistors With Graphene/Metal Heterocontacts. *IEEE Electron Device Lett.* **2014**, *35*, 599–601.
- (24) Baek, S. C.; Seo, Y.-J.; Oh, J. G.; Albert Park, M. G.; Bong, J. H.; Yoon, S. J.; Seo, M.; Park, S.; Park, B.-G.; Lee, S.-H. Alleviation of Fermi-Level Pinning Effect at Metal/Germanium Interface by the Insertion of Graphene Layers. *Appl. Phys. Lett.* **2014**, *105*, 73508.
- (25) Chanana, A.; Mahapatra, S. Prospects of Zero Schottky Barrier Height in a Graphene-Inserted MoS₂-Metal Interface. *J. Appl. Phys.* **2016**, *119*, No. 014303.
- (26) Chee, S.-S.; Seo, D.; Kim, H.; Jang, H.; Lee, S.; Moon, S. P.; Lee, K. H.; Kim, S. W.; Choi, H.; Ham, M.-H. Lowering the Schottky Barrier Height by Graphene/Ag Electrodes for High-Mobility MoS₂ Field-Effect Transistors. *Adv. Mater.* **2019**, *31*, No. 1804422.
- (27) Su, J.; Feng, L.; Zeng, W.; Liu, Z. Designing High Performance Metal–mMoS₂ Interfaces by Two-Dimensional Insertions with Suitable Thickness. *Phys. Chem. Chem. Phys.* **2016**, *18*, 31092–31100.
- (28) Kresse, G.; Furthmüller, J. Efficiency of Ab-Initio Total Energy Calculations for Metals and Semiconductors Using a Plane-Wave Basis Set. *Comput. Mater. Sci.* **1996**, *6*, 15–50.
- (29) Kresse, G.; Joubert, D. From Ultrasoft Pseudopotentials to the Projector Augmented-Wave Method. *Phys. Rev. B* **1999**, *59*, 1758–1775.
- (30) Kresse, G.; Furthmüller, J. Efficient Iterative Schemes for Ab Initio Total-Energy Calculations Using a Plane-Wave Basis Set. *Phys. Rev. B* **1996**, *54*, 11169–11186.
- (31) Blöchl, P. E. Projector Augmented-Wave Method. *Phys. Rev. B* **1994**, *50*, 17953–17979.
- (32) Perdew, J. P.; Burke, K.; Ernzerhof, M. Generalized Gradient Approximation Made Simple. *Phys. Rev. Lett.* **1996**, *77*, 3865–3868.
- (33) Monkhorst, H. J.; Pack, J. D. Special Points for Brillouin-Zone Integrations. *Phys. Rev. B* **1976**, *13*, 5188–5192.
- (34) Grimme, S.; Ehrlich, S.; Goerigk, L. Effect of the Damping Function in Dispersion Corrected Density Functional Theory. *J. Comput. Chem.* **2011**, *32*, 1456–1465.
- (35) Moellmann, J.; Grimme, S. DFT-D3 Study of Some Molecular Crystals. *J. Phys. Chem. C* **2014**, *118*, 7615–7621.
- (36) Hamann, D. R. Optimized Norm-Conserving Vanderbilt Pseudopotentials. *Phys. Rev. B* **2013**, *88*, No. 85117.
- (37) Schlipf, M.; Gygi, F. Optimization Algorithm for the Generation of ONCV Pseudopotentials. *Comput. Phys. Commun.* **2015**, *196*, 36–44.
- (38) Stradi, D.; Jelver, L.; Smidstrup, S.; Stokbro, K. Method for Determining Optimal Supercell Representation of Interfaces. *J. Phys. Condens. Matter* **2017**, *29*, 185901.
- (39) Sang, D. K.; Ding, T.; Wu, M. N.; Li, Y.; Li, J.; Liu, F.; Guo, Z.; Zhang, H.; Xie, H. Monolayer β -Tellurene: A Promising p-Type Thermoelectric Material via First-Principles Calculations. *Nanoscale* **2019**, *11*, 18116–18123.
- (40) Park, J. Y.; Joe, H.-E.; Yoon, H. S.; Yoo, S.; Kim, T.; Kang, K.; Min, B.-K.; Jun, S. C. Contact Effect of ReS₂/Metal Interface. *ACS Appl. Mater. Interfaces* **2017**, *9*, 26325–26332.
- (41) Tang, H.; Shi, B.; Pan, Y.; Li, J.; Zhang, X.; Yan, J.; Liu, S.; Yang, J.; Xu, L.; Yang, J.; Wu, M.; Lu, J. Schottky Contact in Monolayer WS₂ Field-Effect Transistors. *Adv. Theory Simulations* **2019**, *2*, No. 1900001.
- (42) Fuentealba, P.; Chamorro, E.; Santos, J. C. Chapter 5 Understanding and Using the Electron Localization Function. In *Theoretical Aspects of Chemical Reactivity*; Toro-Labbé, A. B. T.-T. Ed.; Elsevier, 2007; *19*, 57–85.
- (43) Doll, K. Calculation of the Work Function with a Local Basis Set. *Surf. Sci.* **2006**, *600*, L321–L325.
- (44) Henkelman, G.; Arnaldsson, A.; Jónsson, H. A Fast and Robust Algorithm for Bader Decomposition of Charge Density. *Comput. Mater. Sci.* **2006**, *36*, 354–360.
- (45) Mulliken, R. S. Electronic Population Analysis on LCAO–MO Molecular Wave Functions. I. *J. Chem. Phys.* **1955**, *23*, 1833–1840.